Cavity-Backed Waveguide Slot Array for Elimination of Second-Order Lobes

Jacob Carl Coetzee, *Senior Member, IEEE*

***Abstract*—Two-dimensional arrays of longitudinal waveguide slots feature non-uniform offsets to achieve the desired element excitations. The irregular element spacing gives rise to second-order beams in the radiation patterns. The unwanted second-order beams inhibit their application in search radar and radiometry applications. Existing techniques for suppression of second-order beams include reducing the slot displacement or collinear alignment by introducing asymmetry in the waveguide. This paper proposes a cavity-backed slot radiator that produces collinear slot arrays. The cavity is fed through a displaced slot between its lower wall and the waveguide branch. The geometry is chosen to restrict the number of variable parameters while maintaining a simple equivalent circuit model. This facilitates the adaptation of the existing design method for conventional arrays that incorporates the various mutual coupling mechanisms to design arrays of cavity-backed slots. The design approach is validated through simulation and measurement of a prototype array.**

***Index Terms*—Waveguide, Antenna arrays, Radar antennas, Slot antennas, Antenna radiation patterns.**

I. Introduction

SECOND-order beams in the radiation patterns of two-dimensional slot array antennas increase the susceptibility of a search radar to jamming or spurious target echoes [1]. Second-order beams can also inhibit the application of these antennas in radiometry, where low average sidelobes are essential [2]. In arrays of longitudinal slots, these beams arise from the non-uniform or alternating displacement of slots with respect to the waveguide branch axes. The secondary beams manifest as grating lobes in the principal planes of the main lobe, or as butterfly lobes in non-principal planes [3].

Second-order beams beams may be suppressed by minimizing slot displacement from the waveguide centerline [4] or ideally, using collinear slots. Collinear alignment may be obtained by using asymmetric ridge waveguide [5], asymmetric posts in conventional waveguide [6], iris-fed and septum-fed slots [7] or corrugated-wall waveguide. Other methods involve the addition of a short section of a truncated waveguide above waveguide slot and radiating in free space [8].

Cavity-backed slots have been used as radiating elements for arrays comprising a combination of 2×2 subarrays. The main objectives of these studies were high-efficiency [9] and bandwidth enhancement [10], [11]. The four slots of each subarray are excited uniformly, and subarrays are fed via a feed network. This geometry limits control over the excitation of individual array elements, thus making it unsuitable for applications where low sidelobes are essential.

School of Electrical Engineering and Robotics, Queensland University of Technology, Brisbane, Queensland 4001, Australia

Manuscript received December 16, 2024

In this paper, we propose an alternative cavity-backed slot radiator for implementation of low-sidelobe, collinear slot arrays. The cavity is fed through a displaced slot between its lower wall and the waveguide branch, and radiates through a slot on the axis of the branch. The geometry is chosen to retain only two variable parameters and a simple shunt equivalent circuit model, similar to conventional radiating slots. The existing synthesis procedure for conventional arrays can consequently be adapted for the design of arrays of cavity-backed slots. The approach accounts for both external and higher-order internal mutual coupling. The method is demonstrated by designing and constructing a prototype array. The performance of the array is assessed through finite element analysis and measurement.

II. Radiation Pattern

Consider the planar array in Fig. 1, consisting of T branches with N longitudinal slots of width w in each branch. The array has a total of $M = N \times T$ slots. Branches are fed via center-inclined coupling slots in the upper wall of the main line. The nth slot of branch t has a length of $L_{t,n}$ and an offset $x_{t,n}$ from the axis of the waveguide. The longitudinal spacing between slots is d_h, while the distance between center lines of neighboring branches is d_e.

Assume that the array is steered in a direction $(\theta, \phi) = (\theta_0, \phi_0)$. With a change of variables to $u = \cos\theta$ and $v = \sin\theta\,\cos\phi$, the expression for the radiated far-field given in

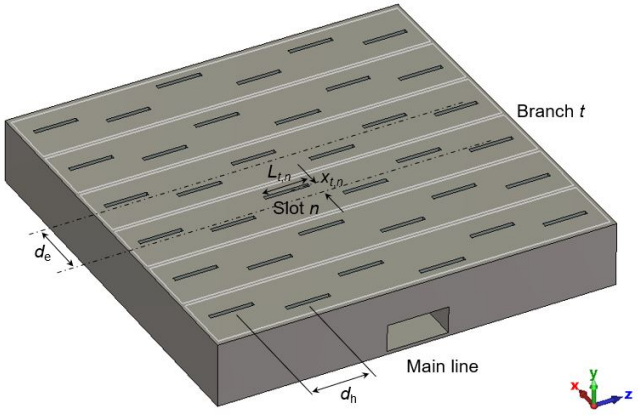

Fig. 1. Geometry of a conventional $T \times N$ planar array.

[12] can be rewritten as

$$E_\phi(u,v) = \sum_{t=1}^{T}\sum_{n=1}^{N}\Big[c_{t,n}\; e^{j2\pi(n-1)(u-u_0)d_h/\lambda_0}\times e^{j2\pi(t-1)(v-v_0)d_e/\lambda_0}\; e^{j2\pi v x_{t,n}/\lambda_0}\; EP_{t,n}\Big]. \quad (1)$$

where $c_{t,n}$ is the excitation amplitude of slot n of branch t. The normalized element pattern of slot n of branch t is given by

$$EP_{t,n} = \text{sinc}(\pi v w/\lambda_0)\times \frac{\cos(\pi u L_{t,n}/\lambda_0) - \cos(\pi L_{t,n}/\lambda_0)}{\sqrt{1-u^2}\,[1-\cos(\pi L_{t,n}/\lambda_0)]}. \quad (2)$$

The term λ_0 in (1) and (2) is the free space wavelength. If the array factor is separable, $c_{t,n} = a_t \times b_n$ where $\mathbf{a} = (a_1\; a_2 \ldots a_T)$ and $\mathbf{b} = (b_1\; b_2 \ldots b_N)$ are the excitation vectors for linear arrays of T and N elements, respectively. To achieve the desired radiation pattern, the complex slot voltages across the width and at the center of each slot should be

$$V^s_{t,n} = c_{t,n} e^{-j2\pi[(n-1)u_0 d_h/\lambda_0 + (t-1)v_0 d_e/\lambda_0]}, \quad (3)$$

thus reducing (1) to

$$E_\phi(u,v) = \sum_{t=1}^{T}\sum_{n=1}^{N}\Big[V^s_{t,n}\; e^{j2\pi[(n-1)u d_h/\lambda_0 + (t-1)v d_e/\lambda_0]}\; e^{j2\pi v x_{t,n}/\lambda_0}\; EP_{t,n}\Big]. \quad (4)$$

The predominant application of two-dimensional slot arrays are narrow-beam, low-sidelobe antennas with the main lobe at broadside, i.e. $\theta_0 = \phi_0 = 90°$. In that case, $E_\phi(0,v)$ corresponds to the E-plane pattern of the array , while $E_\phi(u,0)$ represents the H-plane pattern. These arrays require slot offsets that alternate on either side of the branch axes, as illustrated in Fig. 1. The element excitations are chosen to achieve the desired beam direction and to meet the sidelobe specifications in the principal planes. This is normally done for the array factor only, i.e. for uniform element spacing and without taking the element pattern into consideration. Inclusion of the element pattern suppresses the sidelobes of the H-plane of the broadside arrays and only affects the sidelobe performance when the main beam is scanned [12]. However, the phase term associated with the slot offsets in (1) or (4) gives rise to the second-order beams.

III. Illustration of Second-Order Lobes in Conventional Slot Arrays

Consider for example a 6×6 array designed at a frequency of 9 GHz and using standard WR90 waveguide with dimensions a = 22.86 mm and b = 10.16 mm for both the main line and the branch lines. The radiating and coupling slots have a width of w = 1.5875 mm, with a waveguide wall thickness of h = 1.27 mm. The radiating slots and the coupling slots are spaced at half the guide wavelength, that is, $d_h = d_e = 24.315\text{mm} = 0.73\lambda_0$. For an array factor with a Chebyshev pattern and 25 dB sidelobes and the main lobe at broadside, the excitation vectors are given as $\mathbf{a} = \mathbf{b} = (0.3865, 0.7267, 1.0, 1.0, 0.7267, 0.3865)$. The procedure described in [13] was used to determine the lengths, offsets and inclination angles of the radiating and coupling slots of the array. As per convention, a total conductance for each of the branches of $g_t = 2$ was selected. The design produced radiating slot lengths ranging between 15.94 and 16.56 mm and the magnitude of slot offsets varying between 1.18 and 4.98 mm.

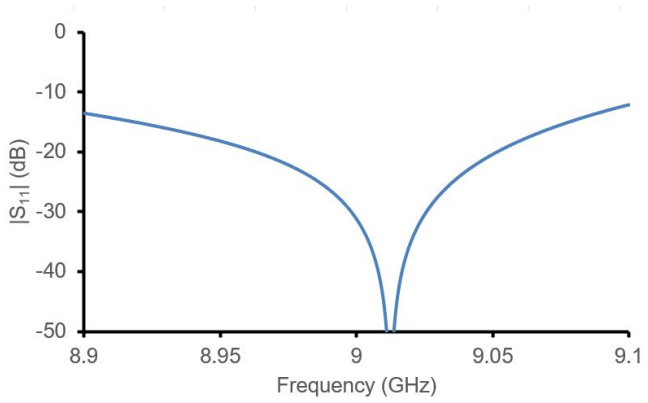

Fig. 2. Reflection coefficient of the conventional 6×6 array slot array.

The array was analyzed using the finite element frequency domain solver of CST Microwave Studio. The return loss performance is shown in Fig. 2. Although minimum reflection is shifted by 0.14% off the design frequency, the array is well matched with a reflection coefficient of less than -30 dB at 9 GHz.

The slot voltages defined in (3) only serve as design objectives during the synthesis process [13]. In reality, modest deviations in amplitude and phase of the implemented array's slot voltages are to be expected. Referring to the geometry shown in Fig. 3, the realized voltage in a slot can be calculated from

$$V^s = \int_{-w/2}^{w/2} E_x(x',0,0)\,dx' \quad (5)$$

or, alternatively,

$$V^s = \frac{2L}{\pi}\int_{-L/2}^{/2}\int_{-w/2}^{w,2} E_x(x',0,z')\,dx'\,dz' \quad (6)$$

where $\mathbf{E}(x',y',z')$ is the electric field obtained from the finite element analysis. The expression in (6) takes the field over the entire aperture into account. It generally produces more reliable results, especially when field sampling is sparse or when the slot field presents a degree of asymmetry. The realized slot voltages $V^s_{t,n}$ can be utilized to calculate the achieved radiation pattern of an array, using (6) and (4).

Fig. 4 shows the radiation pattern for a fictitious array with identical slot lengths as per the design, but with the slot offsets $x_{t,n}$ set to zero. The shaded parts of the surface plot indicate angular regions where the normalized radiated power exceeds the sidelobe level of -25 dB. As expected, this only includes the main lobe centered at $u_0 = v_0 = 0$. The E-plane pattern shows the conventional Chebyshev response with

uniform -25 dB sidelobes, while the progressive suppression of the sidelobes in the H-plane is due to the element pattern having a maximum at $u = 0$ and nulls at $u = \pm 1$. In angular regions off the pricipal planes, the radiated power is below -50 dB relative to the peak of the main lobe. Fig. 4 represents the ideal pattern, and practical designs aim to achieve one that resembles it.

In contrast, the emergence of second-order lobes are apparent when the additional phase term associated with the non-uniform and alternating slot offsets in (4) is included. Fig. 5 shows the radiation pattern of the actual array with non-zero slot offsets. The following observations apply:

- In the H-plane, the array still meets the sidelobe specification and no second-order lobes are observed.
- In the E-plane, secondary grating lobes are present at $v = \pm 1$. The mean element spacing in the E-plane of $d_e = 0.73\lambda_0$ is within the upper limit of $d_{\max} = 0.79\lambda_0$ [12], but the second-order lobes result from the irregular element spacing. For relaxed sidelobe specifications or larger arrays, the grating lobes could potentially be suppressed by employing the approach described in [12] to adjust the excitation vector $\mathbf{a}$. However, for this combination of array size and sidelobe level, it was not feasible.
- In angular regions off the principal planes, radiated power is elevated, and in some directions close to the H-plane, second-order lobes exceed the specified sidelobe level. This undesirable phenomenon is caused by the irregular array geometry and cannot be compensated for through adjustment of element excitations. The only feasible option for suppression of second-order radiation is to reduce the slot displacement from the branch axes, or to change the feed structure to accommodate collinear slots.

IV. CAVITY-BACKED SLOT RADIATING ELEMENT

We propose a new radiating element comprising an offset cavity with a displaced cavity slot between its lower wall and the waveguide branch, and in its upper wall, a radiating slot centered on the branch axis. An exploded view of the radiating element is shown in Fig. 6. Using the axis of the branch guide as reference, the centerline of the cavity slot is laterally displaced by a distance x^{cav}. The cavity of dimensions $a^{\text{cav}} \times b^{\text{cav}} \times c^{\text{cav}}$ has a lateral displacement of $x^{\text{cav}}/2$ and the radiating slot has zero displacement. The cavity and radiating slots have identical width w, but distinct lengths L^{cav} and L^{rad}. The wall thickness of the layers containing the radiating and

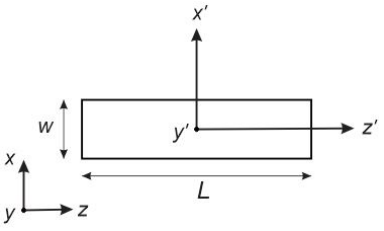

Fig. 3. Geometry of a slot with the origin of a local coordinate system at the center of the aperture.

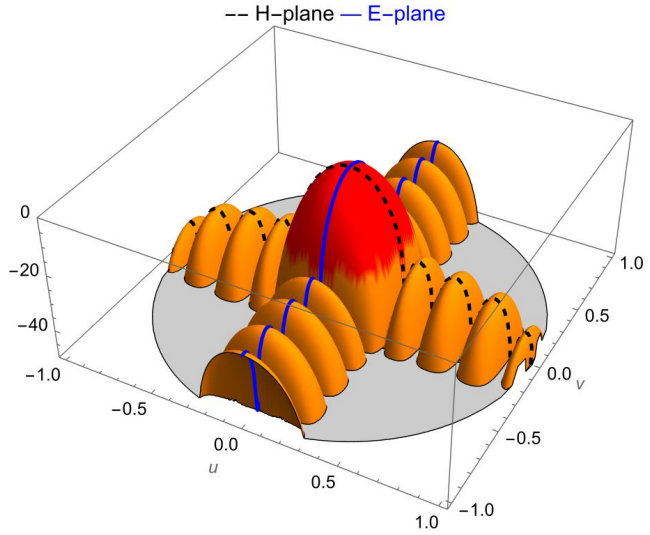

Fig. 4. Normalized radiation pattern of a fictitious array with uniform slot spacing in both the longitudinal and transverse directions.

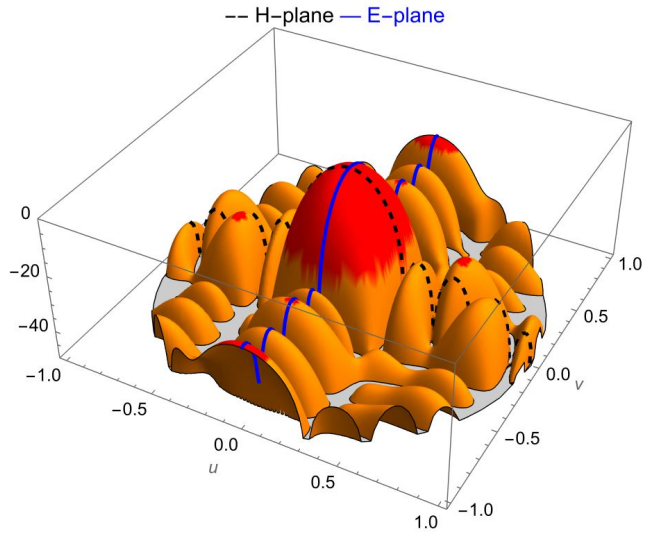

Fig. 5. Normalized radiation pattern of the conventional array with effects of alternating slot offsets included.

cavity slots is h. The cavity slot offset and cavity displacement can be varied to control the power coupled into the cavity, while the radiating slot remains stationary.

The radiating element was analyzed at a frequency of 9 GHz using CST Microwave Studio to determine its scattering parameters. The values for a, b, w and h were kept to those used in Section III. For conventional narrow-beam slot arrays, radiating slots typically have lengths ranging between $0.47\lambda_0$ and $0.49\lambda_0$. We therefore selected a consistent length $L^{\text{rad}} = 15.9$ mm $\approx 0.48\lambda_0$ for the radiating slot. Compact cavity dimensions of $a^{\text{cav}} = 14$ mm, $b^{\text{cav}} = 3$ mm and $c^{\text{cav}} = 20$ mm were chosen to accommodate the range of cavity slot offsets while avoiding overlapping cavities when applied as radiating element in an array. The T-network equivalent circuit elements were computed in terms of the scattering parameters. It was found that the shunt equivalent circuit

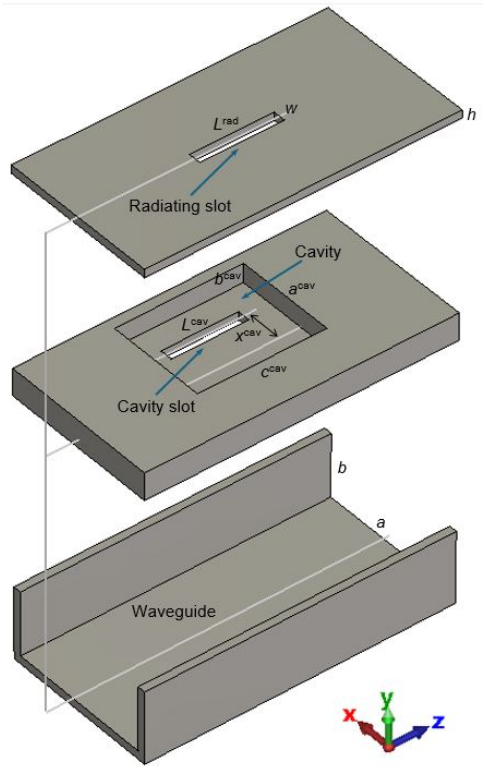

Fig. 6. Explored view of the cavity-backed slot radiating element.

approximation holds for the cavity-backed slot radiator. The normalized self-admittance $y^{\text{self}} = \frac{1}{2}[(1-S_{11})^2 - S_{11}^2]/S_{21}$ was calculated for cavity slot offsets x^{cav} ranging from 0.8 to 5 mm and lengths L^{cav} from 15 to 17 mm. We identified the resonant length for each offset where $y^{\text{self}} = g^r + j0$, and compared the resonant slot conductance g^r with the corresponding values obtained for conventional longitudinal slots. The results in Fig. 7 show close agreement for smaller offsets, but the cavity-backed radiator produced lower values of conductance in the upper ranges of slot offsets. However, a substantial range of conductance can still be realized, which is vital for the ability to produce an assortment of element excitations. The results suggest that the radiator would be suitable for implementation in an array, provided that the values for total branch conductance are reduced.

In addition to creating a database for $y^{\text{self}}(x^{\text{cav}}, L^{\text{cav}})$, we also compute the slot voltage ratio

$$\rho(x^{\text{cav}}, L^{\text{cav}}) = \frac{V^{\text{rad}}}{V^{\text{cav}}}, \tag{7}$$

where V^{rad} and V^{cav} are the radiating and cavity slot voltages computed from (6) and utilizing the electric field results obtained during the finite element analysis for each sample of $(x^{\text{cav}}, L^{\text{cav}})$. The ratio provides a suitable estimate for the amplitude and phase relationship in the excitation of the radiating and cavity slots for each radiating element of an array. The data for y^{self} and ρ can be interpolated to yield results for arbitrary cavity slot dimensions within the sample range.

V. ARRAY DESIGN

A. Feeding mechanism

Fig. 8 demonstrates the proposed feeding mechanism for an array of cavity-backed slots. Fig. 8(a) shows a shorted main line with inclined coupling slots centered at the magnetic field standing wave maxima. The alternating inclination angles excite the branch lines in-phase and with appropriate power levels. Due to the ends of the branch lines being shorted, standing waves in the branch lines ensue. Cavity slots centered at the peaks of the electric field standing wave maxima in the branch lines couple power into the cavities, as shown in Fig. 8(b). In turn, the cavity fields excite the radiating slots with a chosen amplitude profile and uniform phase, as shown in Fig. 8(c). The objective is to formulate a design method that achieves the desired excitations for radiating slots while ensuring an impedance match at the input of the main line.

B. Design equations

The equivalent circuit for branch t shown in Fig. 9 consists of shunt elements with $y^a_{t,n}$, representing the normalized active admittances of radiating element n. The voltage across $y^a_{t,n}$ is denoted as $V_{t,n}$. This array element has a cavity slot offset $x^{\text{cav}}_{t,n}$ and length $L^{\text{cav}}_{t,n}$. Elliott's first design equation [14] still applies, but here it establishes a relationship between $y^a_{t,n}$, $V_{t,n}$ and $V^{\text{cav}}_{t,n}$. It is given by

$$y^a_{t,n} = K_1 f_{t,n} \frac{V^{\text{cav}}_{t,n}}{V_{t,n}} \tag{8}$$

with the constant K_1 given in [13]. The term $f_{t,n}$ is also available from [13], but with the substitutions $(x^{\text{off}}_{t,n} \rightarrow x^{\text{cav}}_{t,n})$ & $(L_{t,n} \rightarrow L^{\text{cav}}_{t,n})$.

Following the formulation described in [13], we assume that the cavity slot voltages of this array element can be expressed as the sum of five components:

- $V^{\text{cav}}_{t,n(1)}$ is due to a TE_{10} mode of amplitude $A^{10}_{t,n}$ within the branch, incident from the left of the cavity slot.
- $V^{\text{cav}}_{t,n(2)}$ is due to a TE_{10} mode of amplitude $D^{10}_{t,n}$ within the branch, incident from the right of the cavity slot.
- $V^{\text{cav}}_{t,n(3)}$ is due to external mutual coupling from other radiating slots.

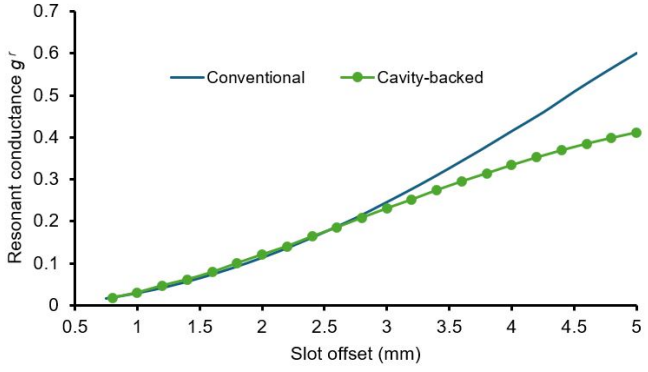

Fig. 7. Resonant slot conductance of the cavity-backed slot radiator as a function of offset compared results for conventional longitudinal slots.

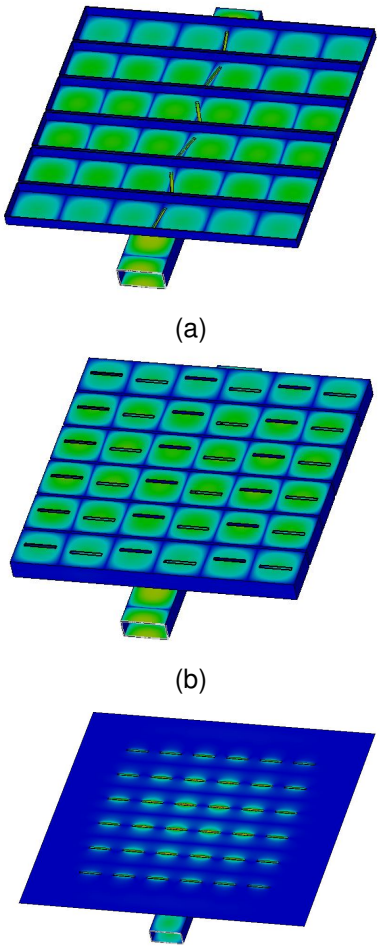

Fig. 8. Electric field distributions in (a) the main line and the branch lines excited by the coupling slots, (b) the cavities fed via the cavity slots in their lower walls, and (c) the radiating slots in the upper walls of the cavities.

- $V^{\text{cav}}_{t,n(4)}$ is due to TE_{20} and TE_{01} mode coupling from neighboring cavity slots.
- $V^{\text{cav}}_{t,n(5)}$ is due to TE_{20} and TE_{01} mode coupling between the cavity slot and inclined coupling slot t, but only for elements neighboring the coupling slot. For all other slots in the branch, this contribution is zero.

The total slot voltage is given by

$$V^{\text{cav}}_{t,n} = \sum_{q=1}^{5} V^{\text{cav}}_{t,n(q)}. \tag{9}$$

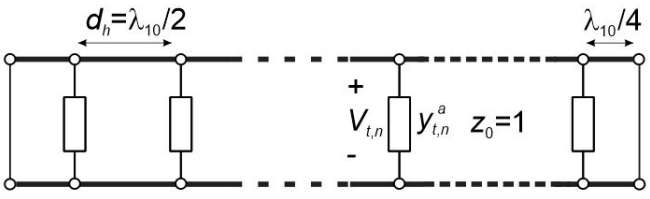

Fig. 9. Equivalent circuit for branch t.

The sum of the first two terms in the expansion of the cavity slot voltage is

$$V^{\text{cav}}_{t,n(1)} + V^{\text{cav}}_{t,n(2)} = \frac{1}{K f_{t,n}} \frac{y^{\text{self}}_{t,n}}{2 + y^{\text{self}}_{t,n}} \left(A^{10}_{t,n} + D^{10}_{t,n}\right) \tag{10}$$

with the constant K given in [13]. Through analysis of the equivalent circuit and substitution of (8), (10) can be rewritten as

$$V^{\text{cav}}_{t,n(1)} + V^{\text{cav}}_{t,n(2)} = V^{\text{cav}}_{t,n} \frac{y^{\text{self}}_{t,n}}{2 + y^{\text{self}}_{t,n}} \frac{2 + y^{a}_{t,n}}{y^{a}_{t,n}}. \tag{11}$$

The remaining slot voltage terms are given by

$$V^{\text{cav}}_{t,n(3)} = -\frac{2}{K_2 f^2_{t,n}} \frac{y^{\text{self}}_{t,n}}{2 + y^{\text{self}}_{t,n}} \sum_{\substack{j=1 \\ j \neq i}}^{M} V^{\text{rad}}_{j} \, g_{ji} \,, \tag{12}$$

$$\begin{aligned} V^{\text{cav}}_{t,n(4)} = &-\frac{2}{K_3 f^2_{t,n}} \frac{y^{\text{self}}_{t,n}}{2 + y^{\text{self}}_{t,n}} \times \\ &\left[V^{\text{cav}}_{t,n-1} \, h^{20}_{t,n} \, h^{20}_{t,n-1} + V^{\text{cav}}_{t,n+1} \, h^{20}_{t,n} \, h^{20}_{t,n+1}\right] \\ &-\frac{2}{K_6 f^2_{t,n}} \frac{y^{\text{self}}_{t,n}}{2 + y^{\text{self}}_{t,n}} \times \\ &\left[V^{\text{cav}}_{t,n-1} \, h^{01}_{t,n} \, h^{01}_{t,n-1} + V^{\text{cav}}_{t,n+1} \, h^{01}_{t,n} \, h^{01}_{t,n+1}\right], \end{aligned} \tag{13}$$

and

$$\begin{aligned} V^{\text{cav}}_{t,n(5)} = &-\frac{2}{K_4 f^2_{t,n}} \frac{y^{\text{self}}_{t,n}}{2 + y^{\text{self}}_{t,n}} V^{\text{cpl}}_{t} \, h^{20}_{t,n} \, p^{20}_{t} \\ &-\frac{2}{K_5 f^2_{t,n}} \frac{y^{\text{self}}_{n}}{2 + y^{\text{self}}_{t,n}} V^{\text{cpl}}_{t} \, h^{01}_{t,n} \, p^{01}_{t} \,. \end{aligned} \tag{14}$$

Constants K_2, K_3, K_4 and K_5 are given in [13] and K_6 in [15]. Mutual coupling terms g_{ji}, $h^{20}_{t,n}$ and $h^{01}_{t,n}$ are defined in [13], but with with substitutions $(x^{\text{off}}_{t,n} \to 0)$ & $(L_{t,n} \to L^{\text{rad}}_{t,n})$ for g_{ji} and $(x^{\text{off}}_{t,n} \to x^{\text{cav}}_{t,n})$ & $(L_{t,n} \to L^{\text{cav}}_{t,n})$ for $h^{20}_{t,n}$ and $h^{01}_{t,n}$. Slot voltage V^{cpl}_{t} and coupling terms $p^{20}_{t,n}$ and $p^{01}_{t,n}$ pertain to the inclined coupling slot between the main line and branch t, and expressions for them are available in [13].

The data for the voltage ratio ρ in (7) is calculated for an isolated radiating element, that is, in the absence of mutual coupling with other elements. We assume that the relation still applies when mutual coupling is included, so that

$$V^{\text{cav}}_{t,n} = V^{\text{rad}}_{t,n} / \rho(x^{\text{cav}}_{t,n}, L^{\text{cav}}_{t,n}). \tag{15}$$

The second design equation provides an expression for the normalized active admittance in terms of its self-admittance and other terms that account for the various forms of mutual

coupling. Substitution of (11), (12), (13) and (14) into (9) yields

$$\begin{aligned}\frac{1}{y^a_{t,n}} =& \frac{1}{y^{\text{self}}_{t,n}} + \frac{1}{K_2 f^2_{t,n}} \sum_{\substack{j=1 \\ j\neq i}}^{M} \frac{V^{\text{rad}}_j}{V^{\text{cav}}_i}\, g_{ji} \\ &+ \frac{1}{K_3 f^2_{t,n}} \left[\frac{V^{\text{cav}}_{t,n-1}}{V^{\text{cav}}_{t,n}}\, h^{20}_{t,n}\, h^{20}_{t,n-1} + \frac{V^{\text{cav}}_{t,n+1}}{V^{\text{cav}}_{t,n}}\, h^{20}_{t,n}\, h^{20}_{t,n+1} \right] \\ &+ \frac{1}{K_6 f^2_{t,n}} \left[\frac{V^{\text{cav}}_{t,n-1}}{V^{\text{cav}}_{t,n}}\, h^{01}_{t,n}\, h^{01}_{t,n-1} + \frac{V^{\text{cav}}_{t,n+1}}{V^{\text{cav}}_{t,n}}\, h^{01}_{t,n}\, h^{01}_{t,n+1} \right] \\ &+ \frac{1}{K_4 f^2_{t,n}} \frac{V^{\text{cpl}}_t}{V^{\text{cav}}_{t,n}}\, h^{20}_{t,n}\, p^{20}_t + \frac{1}{K_5 f^2_{t,n}} \frac{V^{\text{cpl}}_t}{V^{\text{cav}}_{t,n}}\, h^{01}_{t,n}\, p^{01}_t. \end{aligned} \tag{16}$$

Note that (16) applies for the two elements adjacent to coupling slot t. For the other elements of the branch, the last two terms on the right hand side of (16) are omitted.

C. Design procedure

The objective of realizing the desired values of $V^{\text{rad}}_{t,n}$ and an impedance match at the input of the main line is achieved by iteratively computing the cavity slot offsets and lengths $(x^{\text{cav}}_{t,n}, L^{\text{cav}}_{t,n})$ and coupling slot inclination angles and lengths (θ_t, l_t) until convergence is achieved. Note that the cavity slot offsets also determine the lateral displacement of the cavities. The steps follow those listed in [13], but with the following exceptions:

- External mutual coupling terms g_{ji} no longer need to be computed during each iterative pass, as the radiating slot positions and lengths are fixed. Instead, g_{ji} terms only need to be calculated once before iterations begin.
- At the start of each iteration, the cavity slot voltages $V^{\text{cav}}_{t,n}$ are calculated from (15), using the most recent results for cavity slot dimensions $(x^{\text{cav}}_{t,n}, L^{\text{cav}}_{t,n})$.
- The set of nonlinear equations to be solved for calculation of the cavity slot offsets and lengths of branch t during each iteration are replaced with the real and imaginary parts of the following expressions:

$$\frac{y^a_{t,n}}{y^a_{t,m_t}} = \frac{-(1)^{n-m_t} f_{t,n} V^{\text{cav}}_{t,n}}{f_{t,m_t} V^{\text{cav}}_{t,m_t}}, \quad 1 \le n \le N,\ n \neq m_t$$
$$\sum_{n=1}^{N} y^a_{t,n} = g_t + j0.$$

  with $y^a_{t,n}$ given by (16). The term m_t represents the index of the reference element and g_t is the total branch admittance.
- The set of nonlinear equations to be solved for calculation of the inclination angles and slot lengths of coupling slots during each iteration are replaced with the real and imaginary parts of the following expressions:

$$\frac{y^a_{t,m_t}}{y^a_{1,m_1}} = \frac{(-1)^{t-1+k_t-k_1+m_t-m_1} f_{t,m_t} V^{\text{cav}}_{t,m_t} \kappa_1}{f_{1,m_1} V^{\text{cav}}_{1,m_1} \kappa_t}, \quad 2 \le t \le T$$
$$\sum_{t=1}^{T} z_t = 1 + j0$$

  where k_t is the index of the first of the two radiating elements of branch t that straddle the coupling slot. The coupling slot impedance z_t and coupling coefficient κ_t are defined in [13].

VI. Prototype Array

A prototype array was designed to the same specifications as in Section III, with cavity dimensions as in Section IV (i.e., $a^{\text{cav}} = 14$ mm, $b^{\text{cav}} = 3$ mm and $c^{\text{cav}} = 20$ mm) and a radiating slot length length of $L^{\text{rad}} = 15.9$ mm. Total slot admittances of $g_1 = g_2 = g_5 = g_6 = 1.25$ and $g_3 = g_4 = 1.4$ yielded a design with a similar range of cavity slot offsets for all branches. The offsets and lengths of the cavity slots together with the inclination angles and lengths of the coupling slots are specified in Table I.

The array was analyzed using the frequency domain solver of CST Microwave Studio. To ensure accuracy in the modeling of slot fields, vacuum blocks were inserted into the volume occupied by the coupling, cavity and radiating slots and a limit of $0.03\lambda_0$ mesh step size was enforced. Adaptive mesh refinement was used to achieve 1% accuracy in the scattering parameters and 0.5% accuracy in port mode impedance calculations. Using the approach described in Section III, the realized radiating slot voltages were calculated and employed to determine the array's radiation pattern. The results at the center frequency are shown in Fig. 10. Due to the regular spacing of the radiating slots, the pattern closely resembles the ideal pattern of Fig. 4. The grating lobes in the E-plane have been eliminated, and secondary lobes in angular regions off the principal planes are suppressed. The array meets the sidelobe specification for all angles outside the main lobe, except for the peaks of the first sidelobes in the H-plane. The off-center frequency radiation patterns at 8.9 GHz and 9.1 GHz are shown in Fig. 11. Sidelobe performance degradation in the H-plane is more pronounced at the higher edge of the frequency band, but the E-plane pattern remains consistent, and suppression of second-order lobes in angular regions off the principal planes is essentially maintained across the band.

The prototype array was also fabricated. The array comprises four layers of aluminum, as shown in Fig. 12. The bottom layer forms the base with threaded holes on one side for attachment of a waveguide-to-coaxial adapter. The second layer houses a single channel that forms the main line and inclined coupling slots in the upper wall of the channel. The third layer has six channels that form the branch lines and six cavity slots in the upper wall of each branch. The top layer contains the offset cavities with a radiating slot in the upper wall of each cavity. Two registration pins at opposite

TABLE I
CAVITY SLOT AND COUPLING SLOT DIMENSIONS

Element index t, n	Cavity slot offset $x^{\text{cav}}_{t,n}$ (mm)	Cavity slot length $L^{\text{cav}}_{t,n}$ (mm)
1,1	0.966	16.384
1,2	-1.703	16.278
1,3	2.722	16.239
1,4	-2.722	16.239
1,5	1.703	16.278
1,6	-0.966	16.384
2,1	0.998	16.234
2,2	-1.816	16.101
2,3	2.717	16.000
2,4	-2.717	16.000
2,5	1.816	16.101
2,6	-0.998	16.234
3,1	1.014	16.225
3,2	-1.772	16.101
3,3	2.668	16.104
3,4	-2.668	16.104
3,5	1.772	16.101
3,6	-1.014	16.225
4,1	1.010	16.224
4,2	-1.763	16.101
4,3	2.709	15.993
4,4	-2.709	15.993
4,5	1.763	16.101
4,6	-1.010	16.224
5,1	0.999	16.235
5,2	-1.820	16.100
5,3	2.696	16.091
5,4	-2.696	16.091
5,5	1.820	16.100
5,6	-0.999	16.235
6,1	0.970	16.385
6,2	-1.710	16.278
6,3	2.697	16.193
6,4	-2.697	16.193
6,5	1.710	16.278
6,6	-0.970	16.385

Slot index t	Coupling slot angle θ_t (degrees)	Coupling slot length l_t (mm)
1	8.6	15.811
2	-17.0	15.826
3	20.8	15.832
4	-20.9	15.832
5	17.0	15.826
6	-8.6	15.811

corners ensure alignment of the layers. The machined layers were joined using twelve bolts through drilled holes in the top three layers and screwed into threaded holes in the base layer, with the assembled structure shown in Fig. 13.

The calculated and measured radiation patterns in the principal planes and at the design frequency of 9 GHz are shown in Fig. 14. The calculated data were taken from the CST simulation. Close agreement is observed between the theoretical and measured results in the H-plane. Some deviations are evident in the sidelobes of the E-plane patterns, but the measured pattern generally meets the sidelobe specifications.

Fig. 15 shows the calculated and measured reflection coefficient of the prototype array versus frequency. Although the measured reflection is generally higher than the theoretical prediction, the -10 dB bandwidth is comparable. In both cases, the minimum reflection is shifted by less than 0.2% off the design frequency, where a measured return loss of 17 dB is indicative of a reasonable impedance match. The simulated and measured gain of the antenna is shown in Table II. The measured results are on average 1.25 dB lower than the theoretical predictions. This trend is attributed to additional losses due to reflection, surface roughness, or imperfect electrical connection between the layers.

TABLE II
CALCULATED AND MEASURED GAIN OF THE PROTOTYPE ARRAY.

Frequency (GHz)	Calculated gain (dB)	Measured gain (dB)
8.9	21.1	19.4
8.925	21.3	19.9
8.95	21.4	20.3
8.975	22.5	20.7
9	22.6	20.9
9.025	22.6	21.2
9.05	22.5	21.6
9.075	22.2	21.5
9.1	21.8	21.5

VII. CONCLUSION

The cavity-backed slot radiator provides a practical solution for suppression of second-order lobes in the radiation pattern of planar arrays. The methodical design approach addresses the effects of mutual coupling on the excitation of individual elements. The method is highly efficient, and only relies on full-wave analysis for the generation of a database for the self-admittance and the slot voltage ratio over a range of typical cavity slot offsets and lengths. The formulation is suitable for implementation on a regular personal computer. With slot data readily available, execution time can typically be measured in minutes or even seconds.

Disparities between the simulated results and the array specifications are ascribed to deviations in the phase of the achieved element excitations, which, in turn, can be attributed to the precision of the engineering approach to approximate the active cavity slot voltages by (15). The approximation makes the design process tractable and relatively easy to apply.

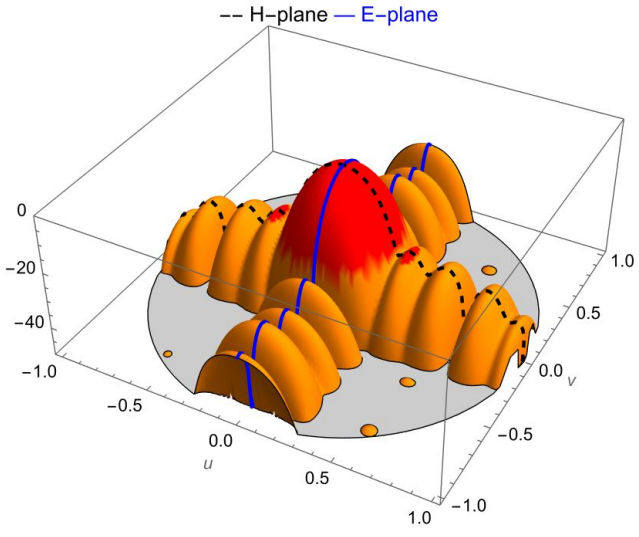

Fig. 10. Radiation pattern of the prototype array with cavity-backed slot elements at the center frequency of 9 GHz.

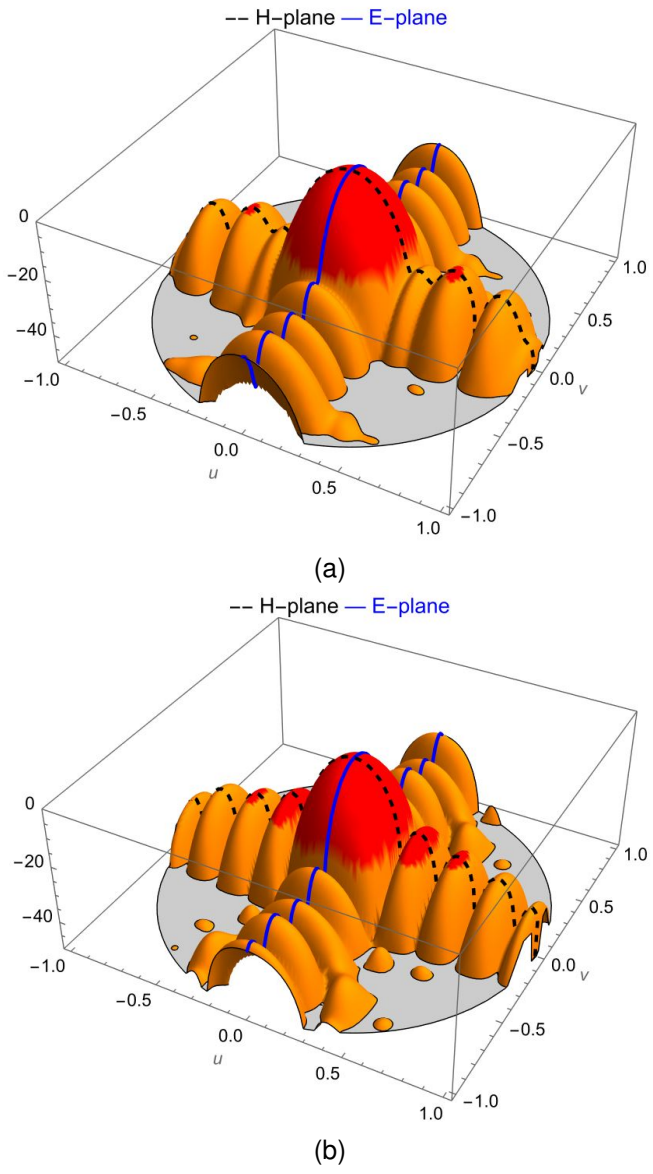

Fig. 11. Off-center frequency radiations patterns at (a) 8.9 GHz and (b) 9.1 GHz.

Its accuracy was assessed by comparing the active cavity slot voltages obtained from the finite element analysis with the approximate values calculated from (15), and the average absolute deviation was found to be 5% in amplitude and 7° in phase.

Discrepancies between the simulated and measured results for the prototype are most likely due to manufacturing tolerances and imperfections. The array was fabricated using CNC milling with a typical tolerance of 10 μm, which is inherently less precise than specialized processes such as laser cutting or spark erosion. The milling process was unable to produce sharp right-angled inside corners for waveguide channels and slots, which consequently had to be radiused by 0.5 mm. In addition, electrical contact between the four metallic layers was only ensured through pressure applied by the perimeter screws, which is less effective than permanent metal-joining processes such as dip-brazing, electron-beam welding, or laser welding.

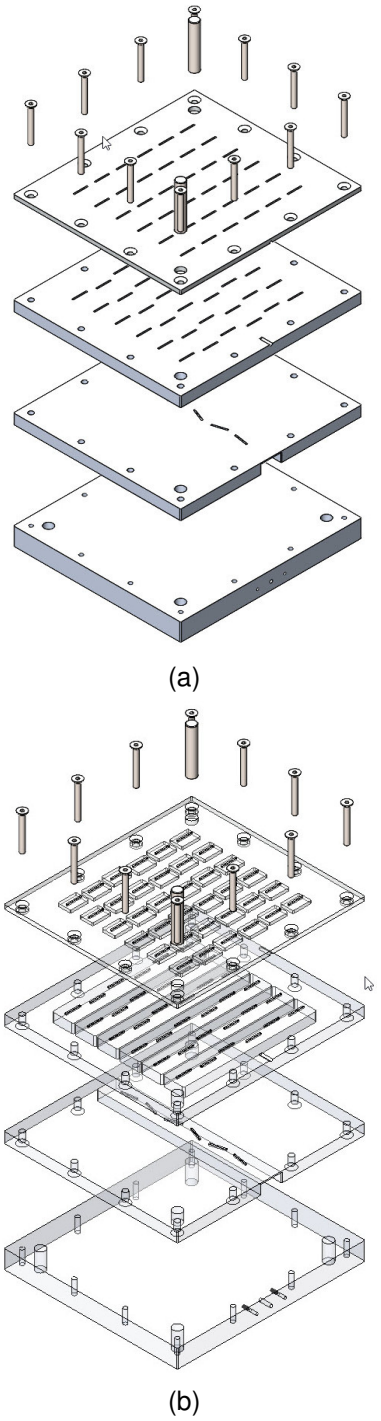

Fig. 12. Exploded view of the prototype array with (a) solid surfaces and (b) transparent surfaces.

However, the practical results successfully demonstrated the viability of the concept and the effectiveness of the proposed design method.

ACKNOWLEDGMENTS

The author would like to thank William Gordon from DeFab, QUT for fabricating the antenna and John Bleddyn from Technical Services, Electrical Engineering, QUT for antenna measurements.

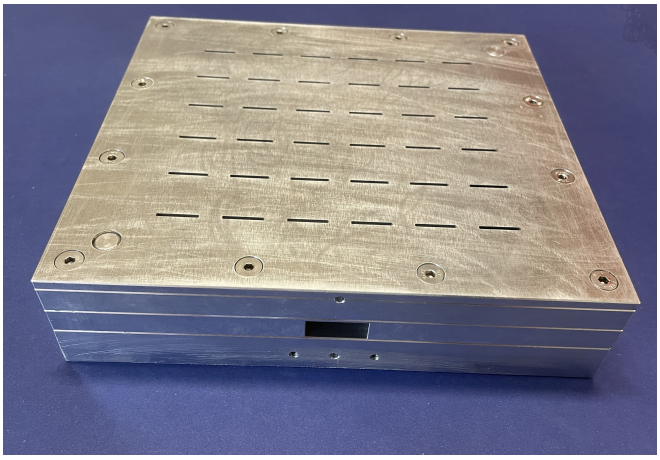

Fig. 13. Assembled prototype array

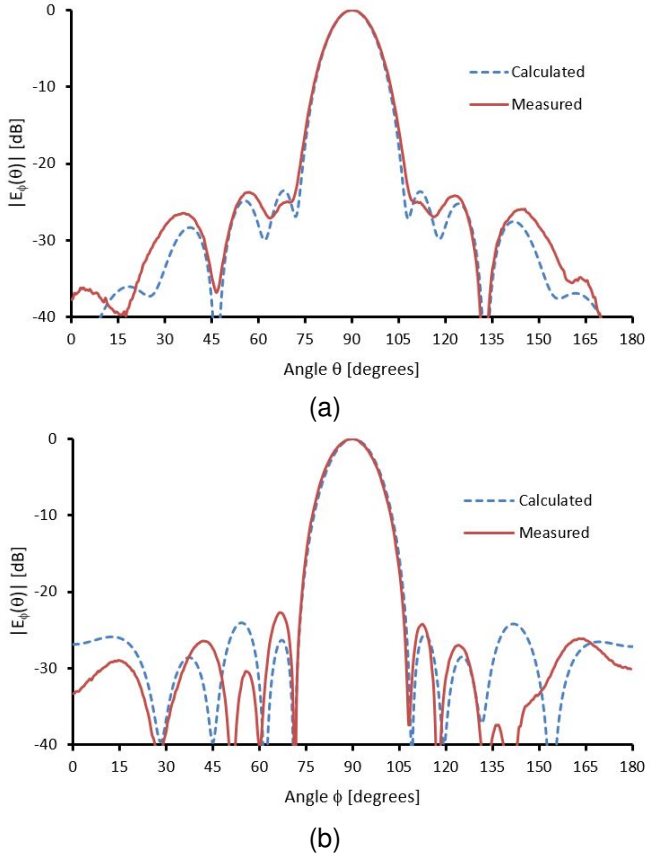

Fig. 14. Calculated and measured radiation patterns of the prototype array at the center frequency in (a) the H plane and (b) the E-plane.

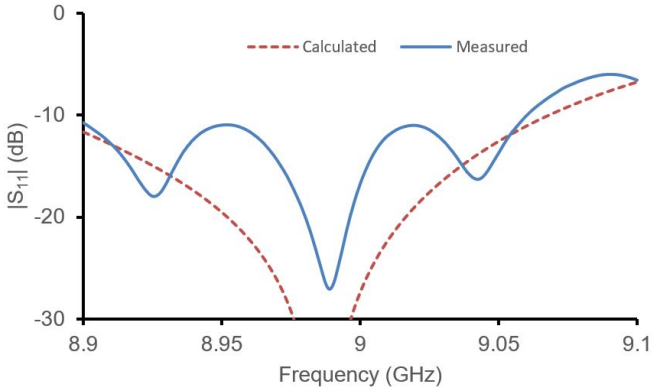

Fig. 15. Calculated and measured reflection coefficient of the prototype array.

REFERENCES

[1] L. Kurtz and J. Yee, "Second-order beams of two-dimensional slot arrays," *IRE Trans. Antennas Propag.*, vol. 5, no. 4, pp. 356-362, Oct. 1957, doi: 10.1109/TAP.1957.1144524.

[2] S. R. Rengarajan, M. S. Zawadzki and R. E. Hodges, "Waveguide-slot array antenna designs for low-average-sidelobe specifications," *IEEE Antennas Propag. Mag.*, vol. 52, no. 6, pp. 89–98, Dec. 2010, doi: 10.1109/MAP.2010.5723227.

[3] A. Derneryd, "Butterfly lobes in slotted waveguide antennas," in *Proc. Antennas Propag. Soc. Int. Sym.*, Blacksburg, VA, USA, 1987, pp. 360–363, doi: 10.1109/APS.1987.1150038.

[4] S. Trinh-Van, S. C. Song, S.-H. Seo and K. C. Hwang, "Grating lobe reduced waveguide slot array antenna," in *Proc. Int. Symp. Antennas Propag.*, Busan, South Korea, 2018, pp. 1–2.

[5] J. Green, H. Shnitkin and P. J. Bertalan, "Asymmetric ridge waveguide radiating element for a scanned planar array, *IEEE Trans. Antennas Propag.*, vol. 38, no. 8, pp. 1161–1165, Aug. 1990, doi: 10.1109/8.56951.

[6] M. Moradian, "Employing irises and septums to excite the centreline longitudinal slot antennas," *Int. J. RF Microw. Comput. Aided Eng.*, vol. 29, pp. 1–12, Sep. 2019, doi:10.1002/mmce.21944.

[7] M. Moradian, "Employing double posts to excite the centerline longitudinal slot antennas," *Microw. Opt. Technol. Lett.*, vol. 62, no. 7, pp. 2618–2628, Mar. 2020, doi: 10.1002/mop.32365.

[8] G. Montisci, G. Mazzarella and G. A. Casula, "Effective analysis of a waveguide longitudinal slot with cavity," *IEEE Trans. Antennas Propag.*, vol. 60, no. 7, pp. 3104–3110, July 2012, doi: 10.1109/TAP.2012.2196953.

[9] G.-L. Huang, S.-G. Zhou and T.-H. Chio, "Waveguide-fed cavity backed slot antenna array with high efficiency in the Ku-band," in *Proc. IEEE Int. Symp. Antennas Propag.*, Chicago, IL, USA, pp. 1–2, 2012, doi: 10.1109/APS.2012.6348586.

[10] W. Y. Yong, A. Haddadi, T. Emanuelsson and A. A. Glazunov, "A bandwidth-enhanced cavity-backed slot array antenna for mm-wave fixed-beam applications," *IEEE Antennas Wireless Propag. Lett.*, vol. 19, no. 11, pp. 1924–1928, Nov. 2020, doi: 10.1109/LAWP.2020.3022988.

[11] J. Liu, A. Vosoogh, A. U. Zaman and J. Yang, "Design and fabrication of a high-gain 60-GHz cavity-backed slot antenna array fed by inverted microstrip gap waveguide," *IEEE Trans. Antennas Propag.*, vol. 65, no. 4, pp. 2117–2122, Apr. 2017, doi: 10.1109/TAP.2017.2670509.

[12] J. C. Coetzee, "Refinements to the design of traveling-vave waveguide slot arrays,"*IEEE Open J. Antennas Propag.*, vol. 5, no. 4, pp. 974–982, Aug. 2024, doi: 10.1109/OJAP.2024.3396501.

[13] J. C. Coetzee and S. Sheel, "Waveguide slot array design with compensation for higher order mode coupling between inclined coupling slots and neighboring radiating slots,"*IEEE Trans. Antennas Propag.*, vol. 67, no. 1, pp. 378–389, Jan. 2019, doi: 10.1109/TAP.2018.2876118.

[14] R. S. Elliott, "An improved design procedure for small arrays of shunt slots,"*IEEE Trans. Antennas Propag.*, vol. 31, no. 1, pp. 48–53, Jan. 1983, doi: 10.1109/TAP.1983.1143002.

[15] J. C. Coetzee and S. Sheel, "Precision design of slot arrays in reduced-height, dielectric-filled or substrate-integrated waveguide using the full T-network equivalent circuit for array elements", *Electromagnetics*, vol. 42, no. 4, pp. 241-254, Aug. 2022, doi: 10.1080/02726343.2022.2110016.

Jacob Carl Coetzee (Senior Member, IEEE) was born in Pretoria, South Africa in 1964. He received the B.Eng. (cum laude), M.Eng. (cum laude) and the PhD degrees in electronic engineering from the University of Pretoria, Pretoria, South Africa in 1987, 1989 and 1994, respectively. He was with the University of Pretoria from 1994 to 1997 and the National University of Singapore, Singapore, from 1998 to 2007. He joined the Queensland University of Technology, Brisbane, Queensland, Australia in 2008. His research interests include analysis and synthesis of microwave circuits, antenna arrays, and smart antennas.